P-associated defects in the high-κ insulators HfO_2 and ZrO_2 revealed by electron spin resonance

A. Stesmans, K. Clémer, and V. V. Afanas'ev
Semiconductor Physics Laboratory, Department of Physics and Institute for Nanoscale Physics and Chemistry (INPAC), University of Leuven, 3001 Leuven, Belgium
(Received 20 March 2007; published 27 March 2008)

We report on the observation by electron spin resonance of P-related point defects in nanometer-thick HfO_2 films on (100)Si after annealing in the range 500–900 °C and in ZrO_2 powder—two oxides prominent in current high-κ insulator research. Based on the principal g matrices and hyperfine tensors inferred from consistent X-, K-, and Q-band spectra simulations and comparison with established P-associated defects in silica, both centers appear similar in nature and are assigned to a P_2-type defect—a P substituting a Hf or Zr atom. Both centers were observed in the monoclinic phase of the high-κ oxides, with the unpaired electron strongly localized on the P atom. Within the concern about dopant penetration out of Si into the high-κ layers on top, identification of the dopant-associated defects in the latter appears crucial to which the present basic results provide fundamental access. The centers may operate as detrimental charge trapping sites.

DOI: 10.1103/PhysRevB.77.125341 PACS number(s): 85.30.De, 73.40.Qv, 61.72.J−, 76.30.Mi

I. INTRODUCTION

Excessive leakage currents encountered in metal-oxide-semiconductor field effect transistors (MOSFETs) as the current conventional unsurpassed a-SiO_2 (SiO_xN_y) gate dielectric is scaled down to the 1 nm range are a main element in the mandatory replacement of the gate insulator by one of higher dielectric constants (κ) [i.e., $\geqslant\kappa(SiO_2)\approx 3.9$].[1] Some of the intensely investigated candidate materials include Al_2O_3, HfO_2, La_2O_3, and ZrO_2, as well as more complicated varieties.[2] The HfO_2-based insulators, more specifically the nitrided Hf silicates ($HfSi_xO_yN_z$), are currently considered as the leading contenders. To serve as a viable candidate, the alternate dielectric must meet stringent requirements. One of these implies superb resistance to dopant penetration during necessary dopant-activation anneals, as this would detrimentally affect device performance. Thus, to be successful, the alternate dielectric should be an excellent diffusion barrier, and, consequently, the behavior of a dopant such as phosphorus is of key interest. Few works have reported on the diffusion of dopants in high-κ dielectrics.[3,4] Alarmingly, with respect to HfO_2-based dielectrics, the results indicated an enhanced penetration of P through HfO_2 or Hf silicates compared with standard SiO_2 films.

Defect sites resulting from P penetration into the high-κ oxides may act as charge traps, whose threat requires attention. Undoubtedly, the assessment of the electrical activity of these defect sites will require information on the atomic scale of how dopants are incorporated into the high-κ network. For this purpose, electron spin resonance (ESR) has been demonstrated to be the preferred technique as evidenced by the reliable identification of numerous (impurity related) point defects in various dielectrics, such as SiO_2. One pertinent class here concerns dopant-associated centers.[5] Indeed, ESR studies of P-associated defects in SiO_2-based glasses resulted in the observation and identification of several defect centers. This may be evident from the overview given in Table I of the different P-associated defect centers so far observed in SiO_2-based glasses[6–10] and P doped c-SiO_2 (Ref. 11) together with the corresponding principal values of the g tensor and hyperfine (hf) matrix.

A. P-associated defects in SiO_2-based materials: Previous results

Uchida *et al.* succeeded in the incorporation of P ions in hydrothermally grown quartz crystals.[11] Upon x or γ irradiation of the doped crystals, ESR measurements performed at ~40, 120, and 290 K revealed three sets of ^{31}P hf lines labeled P(I), P(II), and P(A), where P(I) and P(II) were observed as separate ESR signals at low temperatures ($T<140$ K) and P(A) appears at high T. It was demonstrated that the three sets of resonances are separate but show related appearances of an unpaired electron localized at a pentavalent P ion that occupies substitutionally a Si site: P(I) is ascribed to the ground state of four-fold coordinated P $[PO_4]^0$, P(II) is the first accessible excited state of P(I), and P(A) is the dynamic average. Based on the symmetry properties, a structural model was proposed, as presented schematically in Fig. 1(a), introducing an appreciable displacement of the P nucleus. Calculations based on density functional theory (DFT) of the hyperfine parameters agree well with the experimental values and also indicate that the incorporation of P in the c-SiO_2 network results in a significant perturbation of the α-quartz structure surrounding the impurity.[12]

Griscom *et al.* reported on the observation of four different ^{31}P doublets in glassy $10P_2O_5$-$90SiO_2$ subjected to x or γ irradiation, which they labeled P_1, P_2, P_4, and phosphorus oxygen hole center (POHC).[6] The nomenclature P_1 and P_2 was taken from Weeks and Bray[13] who studied P-associated defects in γ-irradiated P_2O_5 and alkali phosphate glasses as these defects appeared to be essentially identical to those observed in P doped SiO_2. The P_1 and P_2 centers are characterized by a very large hf splitting ($A_{iso}\sim 910$ and ~1200 G, respectively (see Table I). The P_1 defect is suggested to be the phosphorus analog of the Si E' center presumably formed by trapping a hole on a threefold coordinated P atom substitutionally occupying a threefolded Si atom at an E' center site. The proposed steric model is shown in Fig. 1(b). The P_2 center appeared to be identical to the $[PO_4]^0$ center reported by Uchida *et al.*[11]

The P_4 and POHC defects both exhibit a much smaller hf splitting than P_1 and P_2 (see Table I). The P_4 center has been

TABLE I. Overview of the literature on the different P-associated defect centers observed in SiO_2-based glasses and P doped c-SiO_2, together with the corresponding principal values of the g and A matrices. Results are obtained at the X-band frequency.

Defect label	Oxide and damage	g	A (G)
P_1	$10P_2O_5$-$90SiO_2$ x or γ irradiated[a]	$g_1=2.002$	$A_1=1030$
		$g_2=1.999$	$A_2=850$
		$g_3=1.999$	$A_3=850$
	PSG films on Si VUV irradiated[b]	$g_1=2.003$	$A_1=989$
		$g_2=1.998$	$A_2=785$
		$g_3=1.998$	$A_3=785$
P_2	$10P_2O_5$-$90SiO_2$ x or γ irradiated[a]	$g_1=2.001$	$A_1=1300$
		$g_2=2.001$	$A_2=1150$
		$g_3=2.001$	$A_3=1150$
	PSG films on Si VUV irradiated[b]	$g_1=2.010$	$A_1=1360$
		$g_2=1.980$	$A_2=1120$
		$g_3=1.980$	$A_3=1120$
P(I), variant of P_2[c]	P-doped α quartz x or γ irradiated[d]	$g_1=2.0012$	$A_1=1228.93$
		$g_2=2.0032$	$A_2=1086.86$
		$g_3=1.9991$	$A_3=1074.84$
P(II), variant of P_2[c]		$g_1=2.0013$	$A_1=1159.72$
		$g_2=2.0034$	$A_2=1025.14$
		$g_3=1.9991$	$A_3=1012.22$
P(A), variant of P_2[c]		$g_1=2.0010$	$A_1=1139.02$
		$g_2=2.0025$	$A_2=1120.99$
		$g_3=2.0003$	$A_3=1057.79$
P_4	$10P_2O_5$-$90SiO_2$ x or γ irradiated[a]	$g_1=2.0014$	$A_1=355.2$
		$g_2=1.9989$	$A_2=-43.8$
		$g_3=1.9989$	$A_3=-43.8$
	PSG films on Si VUV irradiated[b]	$g_1=2.016$	$A_1=274.5$
		$g_2=1.9989$	$A_2=-43.5$
		$g_3=1.9989$	$A_3=-43.5$
$POHC^s$	$10P_2O_5$-$90SiO_2$ x or γ irradiated[a]	$g_1=2.0179$	$A_1=54$
		$g_2=2.0097$	$A_2=52$
		$g_3=2.0075$	$A_3=48$
	PSG films on Si x-ray irradiated[e]	$g_1=2.0185$	$A_1=54$
		$g_2=2.0115$	$A_2=49$
		$g_3=2.0082$	$A_3=47$
$POHC^m$	PSG films on Si x-ray irradiated[e]	$g_1=2.0514$	$A_1=55$
		$g_2=2.0079$	$A_2=50$
		$g_3=2.0032$	$A_3=44$

[a]See Refs. 5 and 6.
[b]Deposited by pressure induced CVD, see Ref. 9.
[c]P(I) is ascribed to the ground state of P_2, P(II) is the first accessible excited state of P(I), and P(A) is the dynamic average. P(I) and P(II) are observed as separate ESR signals at low temperatures ($T<140$ K) and P(A) appears at high T (Ref. 11).
[d]See Ref. 11.
[e]Deposited by subatmospheric CVD, see Ref. 10.

suggested to also originate from the threefold coordinated P precursor site such as P_1 but is formed by trapping an electron, as depicted in Fig. 1(c). Two different variants of the

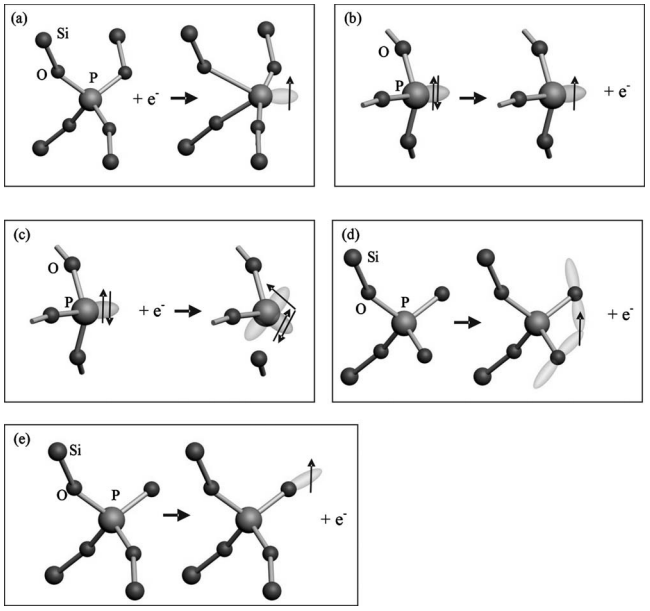

FIG. 1. Overview of the conceptual models proposed in literature for the formation of P-associated defects in SiO_2-based glasses: (a) P_2 (Ref. 11), (b) P_1 (Ref. 6), (c) P_4 (Ref. 6), (d) $POHC^s$ (Ref. 6), and (e) $POHC^m$ (Ref. 6).

POHC were observed: a stable variant ($POHC^s$) and a metastable variant ($POHC^m$) only observed at low temperatures ($T \leqslant 300$ K). The $POHC^s$ was fully characterized and suggested to be a hole trapped on a pair of nonbridging oxygens bonded to the same phosphorus [see Fig. 1(d)]. The $POHC^m$ was tentatively assigned to a hole metastably trapped on the lone nonbridging oxygen bonded to a substitutional P atom, as depicted in Fig. 1(e).

The P-associated defect centers have not only been observed in bulk P doped silica glass but also in thin films of SiO_2-based glasses on Si.[7–10] Warren *et al.* observed the $POHC^s$ in phosphosilicate glass (PSG) and borophosphosilicate glass (BPSG) dielectrics deposited on Si by chemical vapor deposition (CVD) subjected to vacuum ultraviolet (VUV), x-ray irradiation, or hole injection.[7] Based on the charge trapping behavior of the defect, a different model was proposed for the $POHC^s$ where the spin active state is positively charged instead of neutral. This alternative model is the same as the model proposed by Griscom *et al.* for the metastable variant of the POHC. Later on, Fanciulli *et al.* rejected this alternate model for the $POHC^s$ and retained the model proposed by Griscom *et al.* based on the combination of DFT calculations and UV-Raman and ESR measurements on PSG films deposited on Si in a single chamber using subatmospheric CVD (550 °C), and subsequently subjected to x-ray irradiation.[10] Both the $POHC^s$ and $POHC^m$ centers were observed and modeled. In a different work, in addition to the $POHC^s$ the P_1 and P_2 centers were observed in atmospheric pressure CVD deposited BPSG films on Si subjected to VUV irradiation, electron, and/or hole injection.[8] The P_1, P_2, and P_4 defect centers have been observed as well in PSG films deposited on Si by pressure induced CVD, after subjection to VUV irradiation.[9] Theoretical work based on DFT

studies showed that the introduction of P impurities in silica introduces defect states in the band gap.[12] In particular, the P_2 defect has been assigned to be a hole trap.[14]

B. P-associated defects in high-κ oxides: The present work

The present work deals with the ESR observation of P-related point defects in two different oxides eminent in the current high-κ dielectric research, i.e., ZrO_2 and HfO_2. In each case, a similar type of defect is observed, the results indicating that the P atoms can be substitutionally incorporated in both the ZrO_2 and HfO_2 networks, resulting in ESR active defect centers exhibiting similar ESR parameters. In both oxides, a ^{31}P hf doublet of large splitting is observed, assigned to a P_2-type defect. The basic parameters of the defect are assessed to retrieve the defect's atomic nature, which might prove essential in understanding their possible charge trapping behavior and, hence, detrimental effect on device performance.

II. EXPERIMENTAL DETAILS

A. Samples

A first set of samples was obtained from 99.96% pure ZrO_2 powder of particle size of <44 μm and a density of 5.89 g cm^{-3} obtained from Alfa Aesar. As main metallic impurities, the powder contains <50 ppm Hf and <25 ppm Al, Fe, P, Si, and Ti. The particles are crystalline and in the monoclinic phase. After an initial observation of P-associated centers by ESR, a second set of samples was obtained, invoking another prominent high-κ oxide, through depositing 100-nm-thick amorphus HfO_2 on p-type (100)Si substrates, using atomic-layer CVD at 300 °C from $HfCl_4$ and HfO_2 precursors. Inherent to this fabrication method is that the HfO_2 films contain 2%–3% H. To boost ESR detectivity, the samples were implanted by P ions to densities of $\sim 10^{15}$ cm^{-2}, with the implantation energy adjusted to attain a midfilm mean projected range. Separate sets of the HfO_2 samples were subjected to postdeposition annealing (PDA) in N_2 (1 atm) for $\sim$30 min at desired temperatures (T_{an}) in the range 300–900 °C. After initial ESR tests, to maximally reveal all defects, the samples were subjected to suitable photon irradiation. All samples were subjected to unbiased VUV irradiation (10 eV photons; flux of $\sim 10^{15}$ cm^{-2} s^{-1}) obtained from a Kr-resonant discharge lamp. The nanometer-thin HfO_2 films were only irradiated for a relatively short period (20 min), while the micrometer-sized ZrO_2 particles needed to be irradiated for days due to the limited penetration depth of the VUV photons and the shadowing of the powder particles. To overcome the latter, the powder was regularly stirred during irradiation. A separate set of ZrO_2 samples was subjected to UV irradiation ($\sim$2–7 eV, obtained from a Xe lamp) for several hours. During UV irradiation, the powder was contained in a continuously rotating quartz holder put in front of the lamp. Possibly, the treatment may additionally unveil strained or weak bonding (bond rupture) and activate diamagnetic precursor sites.[15]

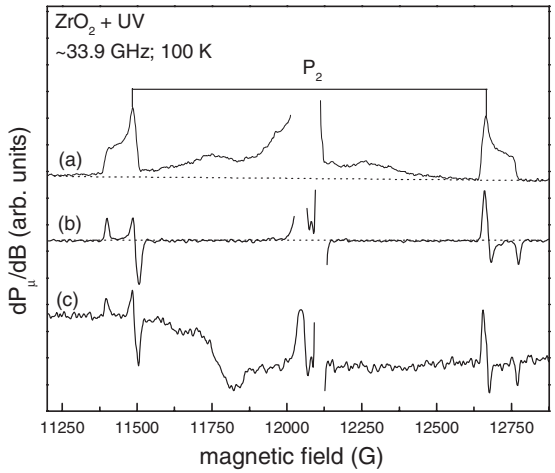

FIG. 2. Q-band ESR spectra of ZrO_2 powder subjected to UV irradiation measured at 100 K: (a) the high-power (saturation) second harmonic mode spectrum, (b) the first derivative of the high-power (saturation) second harmonic mode spectrum, and (c) the conventional low-power derivative-absorption mode spectrum.

B. Electron spin resonance spectroscopy

Initial conventional cw absorption derivative (dP_μ/dB, where B is the magnetic field) Q-band ($\sim$34 GHz, Bruker EMX) ESR measurements[15] were performed at 100 K on the ZrO_2 powder. The modulation amplitude (B_m) of the applied magnetic field and the incident microwave power (P_μ) were restricted to levels not causing (noticeable) signal distortion. A comounted Si:P marker sample [g(100 K)=1.998 91] or a Li:F marker sample (g=2.002 29) was used for g factor and (spin) density calibration. The latter was attained through orthodox double numerical integration of the recorded first-derivative absorption spectra of the defect and the marker. However, to circumvent saturation, in this way increasing sensitivity, the rest of the ESR measurements were performed in the second harmonic mode[16] in X ($\sim$9.2 GHz), K ($\sim$20.4 GHz), and Q bands in the temperature range 4.2–300 K using relatively high modulation amplitudes and microwave powers. As outlined elsewhere, it appears that when appropriate conditions are met for a certain defect center, the second harmonic phase-quadrature (out-of-phase) spectra are identical to the absorption spectra of that defect.[8,15]

III. RESULTS

Curve (a) in Fig. 2 shows a typical high-power second harmonic mode Q-band ($\sim$34 GHz) spectrum observed in 99.96% pure ZrO_2 powder of particle size of <44 μm subjected to UV irradiation. Various signals appear,[17] but in this work we will only focus on the pair of resonance features (doublet) labeled P_2 in Fig. 2. The doublet was observed in the as-received particles but became much more prominent upon VUV or UV irradiation. The doublet could be detected in both the high-power second harmonic mode [Figs. 2(a) and 2(b)] and the conventional low-power derivative-absorption mode [Fig. 2(c)]. After taking the first derivative

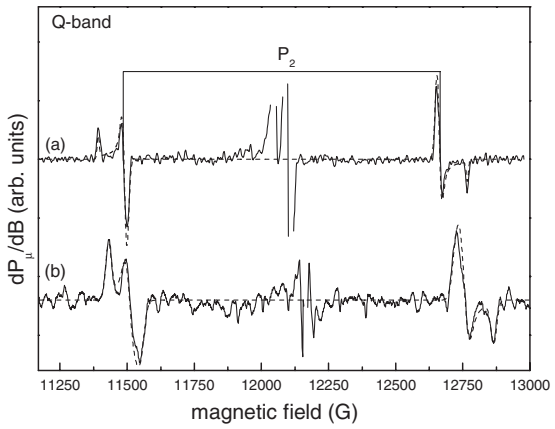

FIG. 3. First derivative of the high-power (saturation) second harmonic mode Q-band spectra (a) measured at 33.91 GHz at 100 K in ZrO_2 powder subjected to UV irradiation and (b) measured at 34.03 GHz at 4.2 K in P-implanted HfO_2 films on Si subjected to a 900 °C postdeposition annealing in N_2 and subsequent VUV irradiation. The dashed curves represent the simulations obtained using the principal g matrix values (a) $g_1=2.0011$, $g_2=2.0007$, and $g_3=2.0007$ and (b) $g_1=1.9965$, $g_2=1.9975$, and $g_3=1.9975$; the principal hf tensor values (a) $A_1=1370$ G, $A_2=1162$ G, and $A_3=1157$ G and (b) $A_1=1425$ G, $A_2=1245$ G, and $A_3=1160$ G, a Gausian line shape; and peak-to-peak line widths (a) $\Delta B^1_{\text{p.p.}}=8$ G, $\Delta B^2_{\text{p.p.}}=17$ G, and $\Delta B^3_{\text{p.p.}}=17$ G and (b) $\Delta B^1_{\text{p.p.}}=24$ G, $\Delta B^2_{\text{p.p.}}=18$ G, and $\Delta B^3_{\text{p.p.}}=24$ G.

of the second harmonic mode spectrum [Fig. 2(b)], identical spectra are obtained in both modes, attesting that both modes can reliably be used to obtain correct ESR parameters (such as the g tensor, hf matrix, and linewidth) of the observed defects. Additionally, the second harmonic mode measurements of the UV irradiated ZrO_2 powder were performed at various (measurement) temperatures T in the range 25–297 K. The observed doublet spectrum did not change, indicating that the ESR parameters are not influenced by the observational temperature.

A similar doublet spectrum was observed in the P-implanted HfO_2 films on Si, but only after subjecting the sample to PDA in the range 500–900 °C followed by VUV irradiation. This is illustrated in Fig. 3(b) showing a representative Q-band spectrum for the HfO_2 sample subjected to PDA at 900 °C, the temperature for which the doublet became the most prominent, and additional VUV irradiation. Moreover, Fig. 3 illustrates that the resonance lines observed in the ZrO_2 powder [spectrum (a)] and in the HfO_2 films are quite similar and, even though the ESR parameters slightly differ, might thus originate from similar defect centers.

Based on the general knowledge of powder pattern ESR line shapes, the kind of symmetry relationship between the two resonance features in one spectrum would leave little doubt about their correlated nature. Yet, to firmly establish whether the two resonance lines do form a natural doublet, complementary X-band (~9.2 GHz) and K-band (~20.4 GHz) ESR experiments were carried out, as illustrated by the spectra shown in Figs. 4 and 5 for the case of (100)Si/HfO_2 and ZrO_2, respectively. It appears that the doublet field splitting slightly increases (~40 G) from X- to

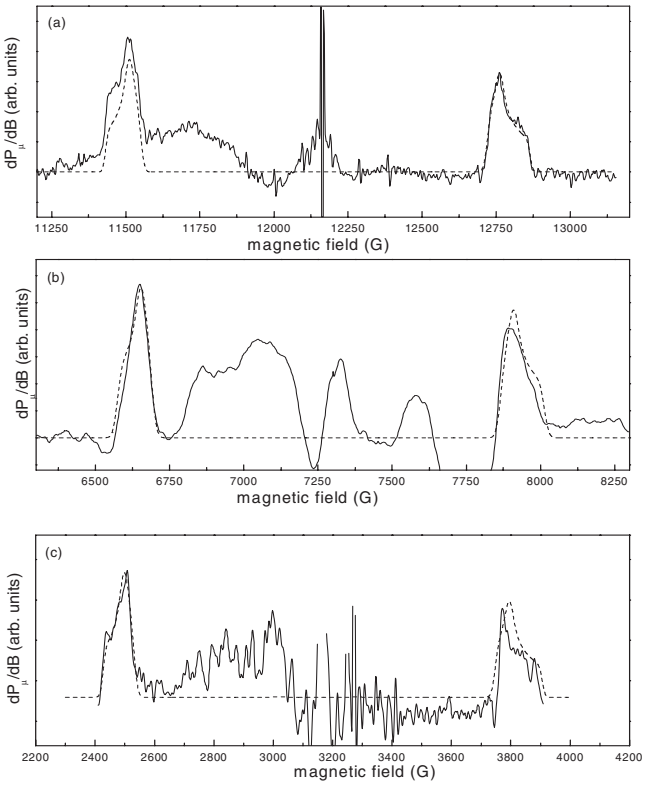

FIG. 4. The high-power (saturation) second harmonic mode Q-, K-, and X-band spectra observed in P-implanted HfO_2 films on Si subjected to a 900 °C postdeposition annealing in N_2 and subsequent VUV irradiation. The dashed curves represent the simulations obtained using, for all three spectra, the principal g matrix values $g_1=1.9965\pm0.0004$, $g_2=1.9975\pm0.0004$, and $g_3=1.9975\pm0.0004$ and the principal hf tensor values $A_1=1425\pm10$ G, $A_2=1245\pm10$ G, and $A_3=1160\pm10$ G.

Q-band measurements, but is in first order independent of the observational frequency. The central g value (g_c) of the doublet, however, shifts significantly downward ($\Delta g_c\sim0.064$) from X to Q band (see Fig. 5). This shift in g_c is found to be consistent with the Breit-Rabi shift[18] expected for a hf doublet resulting from a $S=\frac{1}{2}$ and $I=\frac{1}{2}$ system exhibiting such large hf splitting (~1200 G), as illustrated in Fig. 6 for the doublet observed in ZrO_2: The experimentally obtained g_c values (filled symbols) for three different microwave frequencies match within experimental error with the variation in g_c values calculated using exact matrix diagonalization for a $S=\frac{1}{2}$ and $I=\frac{1}{2}$ spin system with $A=1160$ G and $g=2.0007$. Furthermore, counter to the common spectral appearance of $S>\frac{1}{2}$ centers, no $\Delta m=2$ transitions (m is the magnetic quantum number) at half magnetic field strength of the $\Delta m=1$ transition could be observed.

IV. ANALYSIS

Altogether, these observations leave little doubt that the two signals concern a hf doublet resulting from the interaction of an unpaired electron of spin $S=\frac{1}{2}$ with a closely 100% naturally abundant nucleus of spin $I=\frac{1}{2}$, rather than stem-

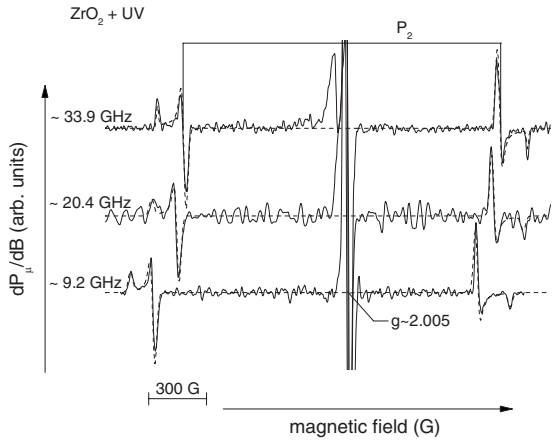

FIG. 5. First derivative of the high-power (saturation) second harmonic mode Q-, K-, and X-band spectra observed in ZrO_2 powder subjected to UV irradiation. The dashed curves represent the simulations obtained using the principal g matrix values $g_1=2.0011\pm0.0004$, $g_2=2.0007\pm0.0004$, and $g_3=2.0007\pm0.0004$ and the principal hf tensor values $A_1=1370\pm10$ G, $A_2=1162\pm10$ G, and $A_3=1157\pm10$ G. The spectra are aligned at the resonance field of a main central signal at $g\sim2.005$ exposing the significant shift of the doublet as a function of observational frequency.

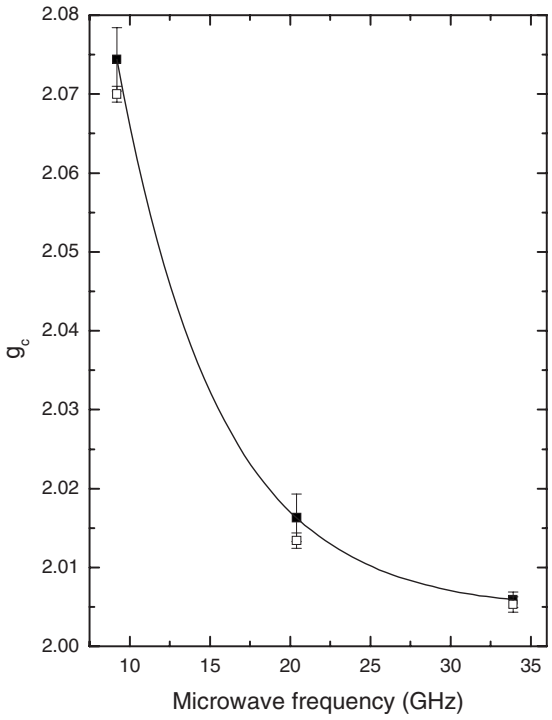

FIG. 6. Zero-crossing g values (g_c) of the measured P_2 signal in ZrO_2 powder subjected to UV irradiation for three different microwave frequencies. Filled symbols: experimentally obtained g_c. Open symbols: calculated g_c obtained using the exact matrix diagonalization for a $S=\frac{1}{2}$ and $I=\frac{1}{2}$ spin system with $A=1160$ G and $g=2.0007$. The solid line is merely meant to guide the eye, exposing the downward shift of the g_c with increasing microwave frequency.

ming from two dissimilar paramagnetic species. In looking for a candidate $I=\frac{1}{2}$ nucleus of 100% natural abundance, which could evoke such large hf splitting ($\sim$1200 G), i.e., large nuclear moment, a quick perusal of the table of isotopes would leave only two possibilities, i.e., ^{31}P or ^{1}H. Taking into account the presence of P impurities in non-negligible amounts ($<$25 ppm) in the ZrO_2 powder and the P-implantation ($[P]\sim10^{15}$ cm^{-2}) signal boost in the HfO_2 samples, ^{31}P follows as the most likely candidate nucleus involved.

The observed doublet spectra, exhibiting typical powder pattern properties, could be consistently described (see Fig. 3, dashed curves) by one effective spin $S=\frac{1}{2}$ and 100% naturally abundant $I=\frac{1}{2}$ center, according to the simplified spin Hamiltonian comprised of the Zeeman and hyperfine terms, respectively,

$$H=\beta\mathbf{B}\cdot\hat{g}\cdot\mathbf{S}+\mathbf{I}\cdot\hat{A}\cdot\mathbf{S}, \quad (1)$$

where $\mathbf{B}$ represents the applied magnetic field, β the Bohr magneton, $\hat{g}$ the g matrix, and $\hat{A}$ the hf tensor for the interaction of the electron spin with a $I=\frac{1}{2}$ nucleus (^{31}P) at one (equivalent) lattice site. For each of the dielectrics separately, the fitting, using a code based on exact matrix diagonalization incorporating the Breit-Rabi formula, could be consistently performed with one set (within experimental error) of $\hat{g}$ and $\hat{A}$ principal values for the independent X-, K-, and Q-band spectra, providing high confidence in the inferred data. The fitting result is illustrated in Figs. 4 and 5 (dashed curves) for the (100)Si/HfO_2 and ZrO_2 case, respectively. The inferred effective $S=\frac{1}{2}$ Hamiltonian parameters are listed in Table II. The indicated experimental accuracies on the inferred g and A values are dominated by the accuracy of the magnetic field sweep since for the wide scans ($>$1000 G), the magnetic field sweep is not perfectly linear. Measurements at three different microwave frequencies and thus in three different experimental setups, however, resulted not only in more reliable spectra simulations but also in a reduction of the experimental error on the ESR parameters.

From the inferred parameters listed in Table II, it may be noticed that the hf doublets observed in ZrO_2 and HfO_2 are quite similar, strongly suggesting that both may originate from nominally the same defect center similarly embedded in a yet different oxide network. Quite naturally, as well expected for a nonidentical environment, some (small) differences in the obtained ESR parameters will emerge, as can be seen from Fig. 3 and Table II. Compared to the HfO_2 case, the defect center observed in the ZrO_2 powder exhibits ESR parameters closer to axial symmetry, the hf splitting is smaller, the principal g values are closer to the free electron g value, and the linewidths are smaller.

Having established pertinent ESR parameters and accepting the P-related nature of the observed defect centers, the next step in the analysis could attempt to assess the structural model. In that search, we are guided by a comparison of our results with ESR data of P-associated defects previously detected in other oxides, in particular those in doped silica glasses.[5–10] A characteristic of the defects observed in the current study is the very large hf splitting, a property only

TABLE II. Comparison of the ESR parameters of the P_2 defect embedded in different oxides. Estimated accuracies on inferred g and A values in this work (see footnotes a and b) are ± 0.0004 and ± 10 G, respectively.

	g_1	g_2	g_3	A_1 (G)	A_2 (G)	A_3 (G)	α^2	β^2	η^2
c-HfO_2[a]	1.9965	1.9975	1.9975	1425	1245	1160	0.27	0.56	0.83
c-ZrO_2[b]	2.0011	2.0007	2.0007	1370	1162	1157	0.26	0.53	0.79
c-SiO_2[c]	2.0012	2.0032	1.9991	1229	1087	1075	0.24	0.37	0.61
a-SiO_2[d]	2.001	2.001	2.001	1300	1150	1150	0.25	0.38	0.63

[a]P_2 in P-implanted HfO_2 subjected to PDA in the range 500–900 °C and VUV (10 eV) irradiation.
[b]P_2 in ZrO_2 powder with $\leqslant$25 ppm P subjected to VUV (10 eV) or UV irradiation (see text).
[c]P(I) variant of P_2 in α quartz subjected to x-ray irradiation (see Ref. 11).
[d]P_2 in P_2O_5-SiO_2 glass subjected to γ-ray or x-ray irradiation (see Refs. 5 and 6).

observed for two types of P-associated defects in SiO_2-based glasses, i.e., P_1 and P_2. Comparing our g and hf data with those from literature (see Tables I and II), the currently observed defects appear to be most similar to the P_2 defect (exhibiting the largest hf splitting) observed in, e.g., P_2O_5-SiO_2 glass[6] and P-implanted α quartz,[11] assigned to a P substituting a Si atom. So, mainly based on a comparison of the Hamiltonian parameters, we assign the currently observed defect centers in HfO_2 and ZrO_2 to P_2-type defects. As already mentioned, in SiO_2 the P_2 center has been ascribed to a P substituting a Si atom: A phosphorus atom of formal oxidation step +5 has taken the place of a silicon atom of oxidation state +4, hereby introducing a "precursor" defect that provides a Coulombic trapping potential for an electron. This model was confirmed by an ESR study of single-crystal P doped α quartz.[11] Based on the observed symmetry properties of the defect, it was suggested that the P_2 defect consists of a P atom back bonded to four O atoms, with the P nucleus considerably displaced. As mentioned before, this model of substitutional P in α quartz has recently been confirmed by theory.[12] Proceeding with the analysis of the observed P_2-type defects, it might be interesting to determine the s (α^2) and p (β^2) character of the orbital composition of the unpaired electron and its localization (η^2) on the central P atom.[5] We might assume that the ground state wave function of P_2 can be approximated by a molecular orbital constructed as the linear combination,

$$|\Psi(x)\rangle = \alpha|\Psi_{3s}\rangle + \beta|\Psi_{3p}\rangle + \sum_i \gamma_i|O_i\rangle, \tag{2}$$

where $|\Psi_{3s}\rangle$ and $|\Psi_{3p}\rangle$ represent the s- and p-state orbitals centered on the P nucleus, and the last term is the sum over all atomic orbitals on nearest-neighbor atoms.[16] In that event, the first two terms on the right hand side are related to observed ^{31}P hf coupling constants through

$$A_1 = A_{iso} + 2b,$$

$$A_2 = A_{iso} - b + c,$$

$$A_3 = A_{iso} - b - c, \tag{3}$$

and $\alpha^2 = A_{iso}/A_s$, $\beta^2 = b/A_p$, and $\eta^2 = \alpha^2 + \beta^2$, where A_s and A_p are, respectively, the atomic s- and p-state hf coupling constants, inferred from theory; the other symbols represent the isotropic (A_{iso}) part (s part: Fermi contact interaction) and the anisotropic (b) part (p part: dipolar interaction) of the hf interaction and the deviation (c) from its perfect sp character. The results of such a linear combination of molecular orbitals (LCMO) analysis are also compared in Table II, together with data on the P_2 defect in silica based glasses and quartz compiled from literature. In each case, the atomic coupling constants calculated for the neutral ^{31}P atom by Morton and Preston[19] were used as those are currently regarded as the most accurate. It should be noted, however, that in previous works, different values for A_s and A_p were used, resulting in different inferred values for α^2 and β^2 from the ones reported in Table II. From the comparison, it appears that the s character of the unpaired electron orbital composition is similar to that for the P_2 center in all oxides, but that the p character is somewhat larger for P_2 in the high-κ oxides than in SiO_2, while the unpaired electron of P_2 in HfO_2 or ZrO_2 is more strongly localized on the central P atom than in SiO_2. Some structural variations are, of course, expected when substitutionally embedding P in different matrices (environments), reflecting in the unpaired electron sp hybrid, which will result in the modification of g and A values.

Next, we may wonder about the fraction of P impurity atoms that ultimately end up as an ESR-active P_2 defect. For the P_2 defects in ZrO_2, an accurate defect density could be obtained as the centers could be detected using conventional first-derivative ESR, giving, after prolonged UV irradiation, a density of $\sim 1 \times 10^{15}$ g^{-1}, which means that at least 1% of the P impurities ($\leqslant$25 ppm, as specified) results in an ESR active point defect. The experimental situation is less favorable for the (100)Si/HfO_2 case since due to excessive saturation and limited amount of sample, the P_2 signal could not be measured using conventional ESR. A quantitative determination of defect densities from second harmonic saturation spectra, however, is not straightforward[8] and requires extreme care. The amplitude of the second harmonic mode spectra depends in a complex way on the relaxation times of the defect centers and on various experimental parameters such as the modulation amplitude, the modulation frequency, and the microwave power.[8] Only via an indirect calibration procedure linking the orthodox first-derivative low-power ESR spectra of P_2 in ZrO_2 with the high-power second har-

TABLE III. Comparison of experimental structural parameters for the monoclinic phase of chemically prepared HfO_2 and ZrO_2 powder taken from Ref. 22, and for the trigonal phase of SiO_2 (e.g., α quartz) taken from Ref. 23. Lattice parameters a, b, and c are in Å.

	a	b	c	Monoclinic angle β
m-HfO_2	5.1156 ± 0.0005	5.1722 ± 0.0005	5.2948 ± 0.0005	$99°11' \pm 0°05'$
m-ZrO_2	5.1454 ± 0.0005	5.2075 ± 0.0005	5.3107 ± 0.0005	$99°14' \pm 0°05'$
h-SiO_2	4.92	4.92	5.41	

monic saturation spectra, an estimate could be made of the P_2 density in the HfO_2 samples along the following procedure: For both the ZrO_2 and the HfO_2 samples, a second harmonic Q-band spectrum was recorded of the doublet using the same experimental parameters. Each second harmonic measurement was immediately followed by a conventional first-derivative measurement of the comounted marker again under the same experimental conditions for both samples. This way, we can determine the quotients can be determined of the intensity of the doublet, obtained through a numerical integration of the second harmonic spectrum, to the intensity of the marker, obtained through a double numerical integration of the first-derivative marker spectrum. Assuming that the relaxation times for P_2-type centers in both high-κ dielectrics are comparable, the ratio of the quotients will be equal to the ratio of the total number of P_2-type defects in the two materials. Knowing the P_2 density in the ZrO_2 sample, this resulted in a total of $\sim 4 \times 10^{13}$ and 9×10^{12} P_2 defects in the ZrO_2 sample subjected to UV irradiation and in the HfO_2 sample subjected to PDA at 900 °C and VUV irradiation, respectively. It appears that the total number of P_2 defects that are actually in the cavity when measuring the HfO_2 sample is more than four times lower than when measuring the ZrO_2 sample, accounting for the lower signal to noise ratio of the HfO_2 spectra (see Figs. 3–5). In this way, for the HfO_2 sample subjected to a PDA at 900 °C and VUV irradiation, an estimated defect density of $\sim 5 \times 10^{12}$ cm^{-2} was obtained, which would indicate that about ~0.5% of the implanted P atoms results in a P_2 defect—a fraction quite comparable with the ZrO_2 case and the case of P_2 in atmospheric pressure CVD deposited BPSG films on Si subjected to VUV irradiation, electron, and hole injection.[8] It should be noted, however, that the inferred defect densities probably concern just lower limits as the VUV or UV irradiation might not have been completely exhaustive in activating precursor sites into the ESR active state.

V. DISCUSSION

In the HfO_2 samples, the P_2 center is only observed after PDA at $T_{an} \geqslant 500$ °C and additional VUV irradiation. The temperature of the necessary "turn-on" PDA step is close to the known onset temperature for the crystallization of the HfO_2 film into a mixture of tetragonal and monoclinic phases, with, notably, the monoclinic phase strongly dominating.[20,21] Hence, we suggest that the crystallization is accompanied by part of the implanted P atoms taking the required substitutional position in a particular crystalline phase. Support for the latter may be inferred from the fact, as observed, that the P_2 center was also found to become more prominent upon annealing at higher temperatures. Indeed, it has been shown that the volume fraction of the tetragonal phase in the HfO_2 film decreases with increasing temperature,[20] the film almost completely converting into the monoclinic phase upon annealing at $T_{an} \sim 900$ °C. Apparently the P_2 defect preferentially appears in the monoclinic phase. For the ZrO_2 powder, no PDA step was necessary to observe P_2. This result is still consistent within the above picture as the as-received ZrO_2 particles are in the monoclinic crystalline phase. Moreover, the P impurities were incorporated during high-temperature particle formation, during which (part of) the P atoms could take a Zr substitutional position.

We thus have reached the result that the P_2 defects observed in both high-κ oxides studied are very similar, and both pertain to the monoclinic oxide phase. Looking deeper, these findings seem well founded as the structural parameters for m-HfO_2 and m-ZrO_2 are almost identical (see Table III).[22] Figure 7(a) illustrates the unit cell for the monoclinic phase. Quite naturally, the small differences in the hf parameters of P_2 in both oxides just reflect the small differences in the structural parameters. Comparing, however, our results with those for P_2 in c-SiO_2,[11] the hf parameters were found to deviate more substantially. This can be seen as originating from the different network structure of the α quartz, i.e., trigonal phase as illustrated in Fig. 7(b).[23] A steric model for the adduced P_2-type defect in HfO_2 is depicted in Fig. 8. Thus, the P_2-type defect may seem ubiquitous to all binary oxide glasses, where the fine details of difference in structure may be addressed by theory.

After a PDA treatment at $T_{an} \geqslant 500$ °C, the P_2 centers in the HfO_2 samples were still found to reside in an ESR inactive state (or, at least, too low an ESR active fraction to enable observation). Irradiation by VUV was required to observe the hf doublet. In the ZrO_2 powder, this activation step was not necessary, but additional VUV or UV irradiation did drastically increase the defect density. A possible reason for the photonic impact is that (part of) the defects are ESR inactive due to the presence of a charge compensator.[11] The VUV or UV irradiation would then cause charge transfer, resulting in the proper ESR active state. However, no evidence was found for the presence of such a charge compensator. A second possibility is that (part of) the centers are left ESR inactive due to binding with H, a well known means of inactivation of, for example, Si dangling bond-type point defect.[24] The VUV or UV photons would then photodissociate H from the passivated defects.[25,26] The latter scenario, at

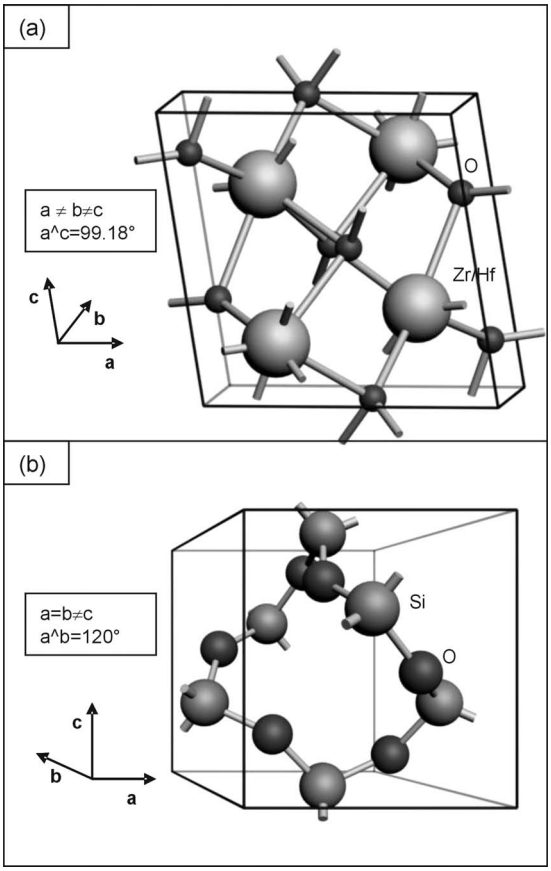

FIG. 7. Illustration of the unit cell of the lattice structure of (a) monoclinic HfO_2 or ZrO_2 and (b) trigonal α quartz.

least partly, is quite likely, especially for the HfO_2 samples as these films contain 2%–3% H as measured by thermal desorption spectroscopy.[27] This would also comply with the lower H content of the ZrO_2 powder.

Having provided evidence that for both high-κ oxides a sizeable fraction ($\sim 0.5\% - 1\%$) of the P atoms results in a P_2 defect, we should draw attention to their potential operation as charge traps, which would make them detrimental for device performance.[3,4,8] There seems little doubt about this: In SiO_2, it has been concluded theoretically as well as experimentally that the P_2 defects act as a hole trap.[9,14] Whether the P_2 defects observed in the current high-κ oxides will also act as hole traps depends on the position of the energy level of the defects in the band gap of the oxides. For this, theory could provide valuable information to eventually

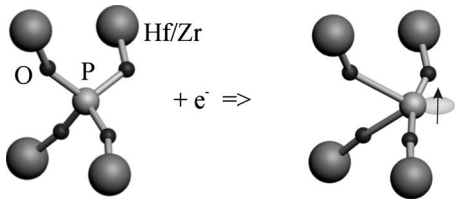

FIG. 8. Proposed conceptual model and the formation of the ESR-active P_2 defect in ZrO_2 and HfO_2.

establish the charge trapping behavior of the P_2 defects embedded in HfO_2 and ZrO_2.[28] The matter becomes even more crucial as recent studies indicate enhanced P diffusion through HfO_2 compared to SiO_2.[3,4]

VI. CONCLUSIONS

In summary, we have reported on the observation by ESR of phosphorus related point defects in two prominent high-κ oxides, i.e., ZrO_2 and HfO_2. These donor related defects exhibit similar ESR parameters and are both assigned to a P_2-type center, largely based on a comparison with the well known P-associated defects in silica. Thus, the defect is ascribed to a P^{4+} atom substituting for Zr or Hf in the monoclinic phase of the ZrO_2 and HfO_2 matrices, respectively, where based on the elemental LCMO analysis, the unpaired electron is found to be strongly localized on the P atom.

A sizeable fraction of the incorporated P impurities was found to result in ESR active P_2-type defects. As these may act as detrimental charge traps in the oxide, the results of recent studies pointing out enhanced P diffusion through HfO_2 compared to SiO_2 may urge one to analyze the latter in more detail to evaluate the potential threat for a MOS-based device operation. This will require correlative studies combining ESR with electrical and optical methods, backed up by theoretical insight.

In search of the replacement of the standard SiO_2 gate insulator in MOSFETs by a high-κ dielectric such as HfO_2, one major obstacle encountered is the generally enhanced trap density in the metal oxide based layer. Along the current results, it appears that (enhanced) migration of dopant impurities resulting in additional traps during necessary dopant-activation thermal steps may add one more element to this concern. The current work represents an initial step in atomically identifying potential charge traps in favored high-κ oxides for device application.

[1] *International Technology Roadmap for Semiconductors* (Semiconductor Industry Association, San Jose, CA, 2005).
[2] G. Wilk, R. M. Wallace, and J. M. Anthony, J. Appl. Phys. **89**, 5243 (2001); J. Robertson, Solid-State Electron. **49**, 283 (2004).
[3] M. A. Quevedo-Lopez, M. R. Visokay, J. J. Chambers, M. J. Bevan, A. Lifatou, L. Colombo, M. J. Kim, B. E. Gnade, and R. M. Wallace, J. Appl. Phys. **97**, 043508 (2005).
[4] K. Suzuki, H. Tashiro, Y. Morisaki, and Y. Sugita, Jpn. J. Appl. Phys., Part 1 **44**, 8286 (2005).
[5] See, e.g., D. L. Griscom, in *Glass: Science and Technology*, edited by D. R. Uhlmann and N. J. Kreidl (Academic, New York, 1990), Vol. 4B, p. 151.
[6] D. L. Griscom, E. J. Friebele, K. J. Long, and J. W. Fleming, J. Appl. Phys. **54**, 3743 (1983).

[7] W. L. Warren, M. R. Shaneyfelt, D. M. Fleetwood, P. S. Winokur, and S. Montague, IEEE Trans. Nucl. Sci. **42**, 173 (1995).
[8] R. Fuller, H. Evans, C. Gamten, B. Czagas, M. Morrison, D. Decrosta, R. Lowry, P. Lenahan, and C. Frye, IEEE Trans. Nucl. Sci. **43**, 2565 (1996).
[9] P. Lenahan, C. A. Billman, R. Fuller, H. Evance, W. H. Speece, D. Decrosta, and R. Lowry, IEEE Trans. Nucl. Sci. **44**, 1834 (1997).
[10] M. Fanciulli, E. Bonera, S. Nokhrin, and G. Pacchioni, Phys. Rev. B **74**, 134102 (2006).
[11] Y. Uchida, J. Phys. Soc. Jpn. **42**, 1937 (1977); Y. Uchida, J. Isoya, and J. A. Weil, J. Phys. Chem. **83**, 3462 (1979).
[12] J. Laegsgaard and K. Stokbro, Phys. Rev. B **61**, 12590 (2000); **65**, 075208 (2002).
[13] R. A. Weeks and P. J. Bray, J. Chem. Phys. **48**, 5 (1968).
[14] J. Robertson, in *Proceedings of Symposium on the Physics and Technology of Amorphous* SiO_2, edited by R. A. B. Devine (Plenum, New York, 1988), p. 91.
[15] See, e.g., D. L. Griscom, Phys. Rev. B **20**, 1823 (1979); T. E. Tsai and D. L. Griscom, J. Non-Cryst. Solids **91**, 170 (1987).
[16] The resonance lines observed in the center region of the spectra have an origin different from the resonance lines labeled P_2 in Fig. 1, as was established from a careful analysis of the saturation behavior and the response to postdeposition annealing of the different resonances.
[17] A. Stesmans, K. Clémer, and V. V. Afanas'ev, Phys. Rev. B **72**, 155335 (2005).
[18] G. Breit and I. I. Rabi, Phys. Rev. **38**, 2082 (1931).
[19] J. R. Morton and K. F. Preston, J. Magn. Reson. (1969-1992) **30**, 577 (1978).
[20] C. Zhao, G. Roebben, M. Heyns, and O. Van Der Biest, Key Eng. Mater. **206**, 1285 (2002).
[21] J. L. Gavartin, A. L. Shluger, A. S. Foster, and G. I. Bersuker, J. Appl. Phys. **97**, 053704 (2005).
[22] J. Adam and M. D. Rogers, Acta Crystallogr. **12**, 951 (1959).
[23] L. Levien, C. T. Prewitt, and D. J. Weidner, Am. Mineral. **65**, 920 (1980).
[24] See, e.g., D. L. Griscom, J. Appl. Phys. **58**, 2524 (1985); A. Stesmans, *ibid.* **88**, 489 (2000).
[25] A. Stesmans and V. V. Afanas'ev, J. Phys.: Condens. Matter **13**, L673 (2001).
[26] R. A. B. Devine and J. Arndt, Phys. Rev. B **42**, 2617 (1990); H. Hosono, Y. Ikuta, T. Kinoshita, K. Kajihara, and M. Hirano, Phys. Rev. Lett. **87**, 175501 (2001).
[27] S. Kimura, K. Iwamoto, M. Kadoshima, Y. Nunoshige, A. Ogawa, T. Nabatame, H. Ota, A. Toriumi, and T. Ohishi, in *Dielectric Films for Future ULSI Devices: Science and Technology* (JSAP, Kawasaki, 2006), p. 126.
[28] K. Xiong, J. Robertson, M. C. Gibson, and S. Clark, Appl. Phys. Lett. **87**, 183505 (2005).